between the local increase of SWA and changes in other movement parameters such as movement time. Therefore, local SWA homeostasis in right parietal areas 40 and 7 is probably related to local neural processes specific to rotation adaptation and to their post-sleep enhancement. We did not find any correlation between the increase in SWA and the mean decrease of directional error at the end of the training session. Instead, we found a high correlation between the increase in SWA and the standard deviation of directional error at the beginning minus the end of training (Fig. 4c; $r = 0.83$, $P < 0.005$). Therefore, subjects who began rotation adaptation with much more variability or 'noise' in directional error compared to the end of training not only displayed a marked local increase in SWA during sleep but also benefited most from sleep.

These findings provide compelling evidence that the electrophysiological marker of sleep homeostasis, SWA, can be selectively induced in circumscribed regions of the cerebral cortex. Thus, they make a strong case for the local regulation of sleep[2,6,19–22] and support a role for sleep at the cellular level[3,23,24]. Moreover, they show that local SWA induction is triggered by a learning task, suggesting that local plastic changes associated with learning may be involved, directly or indirectly. Finally, they show that local SWA homeostasis is strongly correlated with improved performance in the task after sleep. This suggests that SWA homeostasis may be related to cellular processes underlying learning rather than to metabolic fatigue or depletion. Thus, together with evidence from intracellular studies[25], our results support the notion that slow oscillations might help synaptic consolidation[25–30] or produce synaptic downscaling and increase signal-to-noise ratios in relevant neural circuits[3]. Most importantly, these results connect two fields that had thus far remained separate—the study of sleep homeostasis and that of sleep and plasticity. □

Received 19 March; accepted 14 May 2004; doi:10.1038/nature02663.
Published online 6 June 2004.

1. Steriade, M. Corticothalamic resonance, states of vigilance and mentation. *Neuroscience* **101,** 243–276 (2000).
2. Borbély, A. A. & Achermann, P. in *Principles and Practice of Sleep Medicine* (eds Kryger, M. H., Roth, T. & Dement, W. C.) 377–390 (W. B. Saunders, Philadelphia, 2000).
3. Tononi, G. & Cirelli, C. Sleep and synaptic homeostasis: a hypothesis. *Brain Res. Bull.* **62,** 143–150 (2003).
4. Ghilardi, M. F. *et al.* Patterns of regional brain activation associated with different forms of motor learning. *Brain Res.* **871,** 127–145 (2000).
5. Ghilardi, M. F., Eidelberg, D., Silvestri, G. & Ghez, C. The differential effect of PD and normal aging on early explicit sequence learning. *Neurology* **60,** 1313–1319 (2003).
6. Finelli, L. A., Borbély, A. A. & Achermann, P. Functional topography of the human nonREM sleep electroencephalogram. *Eur. J. Neurosci.* **13,** 2282–2290 (2001).
7. Nichols, T. E. & Holmes, A. P. Nonparametric permutation tests for functional neuroimaging: a primer with examples. *Hum. Brain Mapp.* **15,** 1–25 (2001).
8. Cohen, Y. E. & Andersen, R. A. A common reference frame for movement plans in the posterior parietal cortex. *Nature Rev. Neurosci.* **3,** 553–562 (2002).
9. Jonides, J. *et al.* Spatial working memory in humans as revealed by PET. *Nature* **363,** 623–625 (1993).
10. Mednick, S. C. *et al.* The restorative effect of naps on perceptual deterioration. *Nature Neurosci.* **5,** 677–681 (2002).
11. Stickgold, R., James, L. & Hobson, J. A. Visual discrimination learning requires sleep after training. *Nature Neurosci.* **3,** 1237–1238 (2000).
12. Walker, M. P., Brakefield, T., Morgan, A., Hobson, J. A. & Stickgold, R. Practice with sleep makes perfect: sleep-dependent motor skill learning. *Neuron* **35,** 205–211 (2002).
13. Fenn, K. M., Nusbaum, H. C. & Margoliash, D. Consolidation during sleep of perceptual learning of spoken language. *Nature* **425,** 614–616 (2003).
14. Maquet, P., Schwartz, S., Passingham, R. & Frith, C. Sleep-related consolidation of a visuomotor skill: brain mechanisms as assessed by functional magnetic resonance imaging. *J. Neurosci.* **23,** 1432–1440 (2003).
15. Karni, A., Tanne, D., Rubenstein, B. S., Askenasy, J. J. & Sagi, D. Dependence on REM sleep of overnight improvement of a perceptual skill. *Science* **265,** 679–682 (1994).
16. Fischer, S., Hallschmid, M., Elsner, A. L. & Born, J. Sleep forms memory for finger skills. *Proc. Natl Acad. Sci. USA* **99,** 11987–11991 (2002).
17. Gais, S., Plihal, W., Wagner, U. & Born, J. Early sleep triggers memory for early visual discrimination skills. *Nature Neurosci.* **3,** 1335–1339 (2000).
18. Smith, C. Sleep states and memory processes. *Behav. Brain Res.* **69,** 137–145 (1995).
19. Vyazovskiy, V., Borbély, A. A. & Tobler, I. Unilateral vibrissae stimulation during waking induces interhemispheric EEG asymmetry during subsequent sleep in the rat. *J. Sleep Res.* **9,** 367–371 (2000).
20. Kattler, H., Dijk, D.-J. & Borbély, A. A. Effect of unilateral somatosensory stimulation prior to sleep on the sleep EEG in humans. *J. Sleep Res.* **3,** 159–164 (1994).
21. Huber, R., Deboer, T. & Tobler, I. Topography of EEG dynamics after sleep deprivation in mice. *J. Neurophysiol.* **84,** 1888–1893 (2000).
22. Krueger, J. M. & Obál, F. Jr A neuronal group theory of sleep function. *J. Sleep Res.* **2,** 63–69 (1993).
23. Tononi, G. & Cirelli, C. Some considerations on sleep and neural plasticity. *Arch. Ital. Biol.* **139,** 221–241 (2001).
24. Cirelli, C., Gutierrez, C. M. & Tononi, G. Extensive and divergent effects of sleep and wakefulness on brain gene expression. *Neuron* **41,** 35–43 (2004).
25. Steriade, M. & Timofeev, I. Neuronal plasticity in thalamocortical networks during sleep and waking oscillations. *Neuron* **37,** 563–576 (2003).
26. Maquet, P. The role of sleep in learning and memory. *Science* **294,** 1048–1052 (2001).
27. Hoffman, K. L. & McNaughton, B. L. Sleep on it: cortical reorganization after-the-fact. *Trends Neurosci.* **25,** 1–2 (2001).
28. Stickgold, R., Hobson, J. A., Fosse, R. & Fosse, M. Sleep, learning, and dreams: off-line memory reprocessing. *Science* **294,** 1052–1057 (2001).
29. Benington, J. H. & Frank, M. G. Cellular and molecular connections between sleep and synaptic plasticity. *Prog. Neurobiol.* **69,** 71–101 (2003).
30. Walker, M. P. A refined model of sleep and the time course of memory formation. *Behav. Brain Sci.* (in the press).

Acknowledgements We thank C. Cirelli, F. Ferrarelli and T. Shakhnovich for their help, colleagues at WISPIC and Columbia for their comments on the manuscript, and R. Davidson and A. Alexander at the Keck Center for support with EEG and MRI facilities. This work was supported by grants from the Swiss Foundation for Fellowships in Biology and Medicine to R.H., from the NINDS to M.F.G, from the National Sleep Foundation to M.M. and from the NIMH to G.T.

Competing interests statement The authors declare that they have no competing financial interests.

Correspondence and requests for materials should be addressed to G.T. (gtononi@wisc.edu).

Resilient circadian oscillator revealed in individual cyanobacteria

Irina Mihalcescu[1], Weihong Hsing[2]* & Stanislas Leibler[3]

[1]*Laboratoire de Spectrométrie Physique, Université Joseph Fourier – Grenoble I, BP87, 38402 St-Martin d'Hères Cédex, France*
[2]*Department of Molecular Biology, Princeton University, Princeton, New Jersey 08544, USA*
[3]*Laboratory of Living Matter and Centre for Studies in Physics and Biology, The Rockefeller University, 1230 York Avenue, New York 10021, USA*

* Present address: Johnson & Johnson PRD, PO Box 300, Raritan, New Jersey 08869, USA

Circadian oscillators, which provide internal daily periodicity, are found in a variety of living organisms, including mammals, insects, plants, fungi and cyanobacteria[1]. Remarkably, these biochemical oscillators are resilient to external and internal modifications, such as temperature and cell division cycles. They have to be 'fluctuation (noise) resistant'[2] because relative fluctuations in the number of messenger RNA and protein molecules forming the intracellular oscillators are likely to be large. In multicellular organisms, the strong temporal stability of circadian clocks, despite molecular fluctuations, can easily be explained by intercellular interactions[3–5]. Here we study circadian rhythms and their stability in unicellular cyanobacteria *Synechoccocus elongatus*. Low-light-level microscopy has allowed us to measure gene expression under circadian control in single bacteria, showing that the circadian clock is indeed a property of individual cells. Our measurements show that the oscillators have a strong temporal stability with a correlation time of several months. In contrast to many circadian clocks in multicellular organisms, this stability seems to be ensured by the intracellular biochemical network, because the interactions between oscillators seem to be negligible.

Cyanobacteria *S. elongatus* sp. PCC7942, chosen for the present study, is among the simplest organisms showing circadian behaviour[6]. Recent investigations of large populations of these prokaryotic cells have shown that the expression of most of their genes is under the control of a circadian clock[7]. To measure circadian gene

expression in a single cell, we used a bacterial luciferase reporter system[8] consisting of two neutral site chromosomal insertions: *psbAI::luxAB* and *psbAI::luxCDE*. This bioluminescence system, which does not require exogenously added aldehyde substrate, had been successfully used to monitor the circadian clock in populations of cyanobacteria. Note that the use of fluorescent reporters, such as green fluorescent protein (GFP), would be very difficult to implement in *S. elongatus* cells, mainly because of their high auto-fluorescence. In addition, the metabolism and circadian clock would be affected by the strong light needed for fluorescent protein excitation[9], and GFP could be 'bleached' by the prolonged light exposure needed for cell growth.

However, detecting and imaging individual bacteria 2.3–6 μm long requires at least 50 times higher sensitivity than previous bacterial population investigations. This approximates to the ratio between the number of cells in the smallest population yet monitored[10] and a single individual. To achieve this sensitivity, we implemented an experimental set-up based on a back-illuminated cooled CCD (charge-coupled device) detection camera with high quantum efficiency (see Methods). Because the light levels obtained from a single cyanobacterium were typically of the order of 10–20 photons per minute per cell, we used relatively long integration times (30 min) to maximize the signal-to-noise ratio without significantly affecting the circadian rhythm. Computerized control of internal light and temperature, and an entirely automated data acquisition system, allowed measurements to be taken over prolonged periods (up to two weeks) under constant conditions.

In favourable conditions, the cyanobacteria can divide as fast as three to four times during a single circadian cycle[10], while keeping a precise circadian rhythm for the growing population. As the circadian rhythm in cyanobacteria is independent of the cell division cycle[11,12], we imposed an average division time of ~23 h (see Methods) by applying moderate illumination. In this way we were able to observe a slow growth of micro-colonies out of single 'progenitor' cells over long time periods. Figure 1 shows an example of such micro-colony growth during the first 5.5 days (1 day = 24 h), monitored by both phase-contrast and bioluminescence microscopy. The inoculated bacterium (marked F in Fig. 1a) grew slowly, without dividing for the first ~1.2 days. Its density of bioluminescence (defined as the total luminescence divided by the cell size, see Methods) clearly oscillated (Fig. 1b) with a well-defined period of 25.4 ± 0.12 h (mean ± s.d.) (Fig. 1f). After 1 day, the cell doubled its size and started to divide. Figure 1c shows the time course of the size of cell F and all its progeny, extracted from the phase-contrast photographs. The measurement of the total size of all cells in the micro-colony (Fig. 1d) showed that the cells were in the exponential growth phase, with an average doubling time of 23.04 ± 0.17 h. The circadian oscillations of the siblings of the progenitor cell are depicted in Fig. 1e. All the siblings (such as four siblings obtained after two divisions of the initial cell, marked F, F1, F2 and F3 in Fig. 1) were oscillating with a striking synchronicity. Each of the cells had a different amplitude of oscillation, but they were characterized by similar period and phase. Figure 1f shows the density of bioluminescence averaged over all progeny. The average oscillation is well described by a simple periodic function, $\langle d(t)\rangle = B + A\cos(2\pi t/T_0 + \varphi_0)$, in which: d represents density of bioluminescence; $\langle d\rangle$, the average over all progeny; t, time; T_0, period; φ_0, initial phase; A, amplitude; and B, the offset. The average oscillation has not only a constant period and phase, but also a constant amplitude. In the same way, we analysed a few other neighbouring micro-colonies derived from individual cells (see Supplementary Information). Similarly, each progeny oscillated synchronously, with the same period for all the cells studied, and with an average phase that was characteristic of each micro-colony.

We quantified roughly the stability of the individual oscillators and their phase dispersion through successive cell divisions. For this we used the average $\langle d(t)\rangle$ and the variance $\sigma_d^2(t) = \langle (d_i(t) - \langle d(t)\rangle)^2\rangle$ of the signals $d_i(t)$ coming from each individual oscillator i studied. Quantitative analysis of relatively short time sequences, which include only a few oscillations, is both difficult and arbitrary. In a simple stochastic model, the bioluminescence signal from each cell can be expressed as $y_i(t) = A_i(t)[b + \cos(\omega_0 t + \varphi_i(t))]$, where the angular frequency ω_0 and the relative offset b are constant. The amplitude $A_i(t)$ and the phase $\varphi_i(t)$ of each oscillator are two random functions: $A_i(t)$ is a stationary gaussian process, with constant average $\langle A(t)\rangle = A$ and standard deviation σ_A, and $\varphi_i(t)$ is a wiener process with a constant mean $\langle \varphi(t)\rangle = \varphi_0$ and a variance growing linearly with time $\sigma_\varphi^2 = Dt$, where D is the diffusion constant[13]. By comparing the theoretical variance for such random oscillators, $\sigma_y^2(t)$, with the experimental variance, we estimated the amplitude noise, $\eta_A = \sigma_A/\langle A\rangle = 0.25 \pm 0.01$, and the phase diffusion constant, $D = 5 \times 10^{-4} \pm 3 \times 10^{-4}$ (h^{-1}) (see Supplementary Information). These estimates confirm that the observed oscillators have relatively large amplitude fluctuations, but remain strongly in synchrony with a correlation time $\tau = 2/D = 166 \pm 100$ days. Stochastic effects in gene expression fluctuations, such as molecular noise, could be at the origin of these fluctuations, and a noise level of

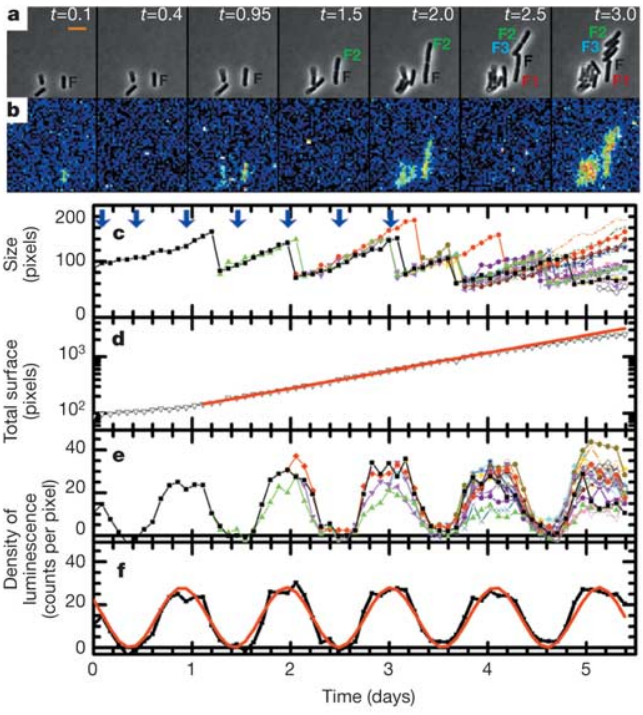

Figure 1 Circadian oscillation of bioluminescence in individual bacteria. **a**, Snapshots of phase-contrast image showing cell F and its progeny and **b**, related bioluminescence image at different times t (given in days, a 24 h period of time) from the beginning of the measurement. Pixels in the bioluminescence images were binned 3 × 3 (pseudo-colour, where red is high signal intensity and blue is low signal intensity). Scale bar, 5 μm. **c**, The size of the cell F and all its progeny as a function of time measured from the phase-contrast images (non-binned pixels). The arrows point to the time where the snapshots in (**a**) and (**b**) were taken. **d**, The total number of pixels occupied by F and its all progeny versus time (black line) plotted in a logarithmic scale. The red line is the corresponding exponential growth fit: total size (t) = initial size × $2^{t/\tau}$ with $\tau = 23.04 \pm 0.17$ h. **e**, Density of bioluminescence for the same cell and all its progeny versus time. **f**, The average density of bioluminescence versus time (black line) and its fit (red line) with: $\langle d(t)\rangle = B + A\cos(2\pi t/T_0 + \varphi_0)$. The resulting period is $T_0 = 25.4 \pm 0.12$ h, the initial phase $\varphi_0 = 52 \pm 2.8°$, the amplitude $A = 12.9 \pm 0.3$ counts per pixel and the offset $B = 14.8 \pm 0.3$ counts per pixel.

gene expression of $\eta = 0.25$ is not unusual[14]. What is surprising is the observed high level of synchronicity. It is tempting to conclude that this stability of oscillations is due to the design of the circadian genetic network in each individual cell. Another possibility, however, is that the individual oscillators become synchronized by coupling one with another. Indeed, many theoretical studies, reinforced by recent experiments[15], have showed that increasing the coupling between noisy—or even chaotic—chemical oscillators results in their synchronization and the establishment of common, robust rhythms.

To test for this possibility, we followed micro-colonies growing in close proximity, but originating from individual cells that had different initial phases of circadian oscillations. Figure 2a presents an example of two such growing micro-colonies, together with the bioluminescence signal showing their out-of-phase circadian oscillations. The 'progenitor' cells, initially separated by ~30 μm, progressively formed two micro-colonies, which after 10–12 successive division cycles got into close contact. Figure 2b depicts the normalized density of bioluminescence of some of the descendants of the two progenitor cells (see Methods). It is quite clear that all the cells from both micro-colonies oscillate with essentially the same period, while their phase is specific to each colony. The phase of the cells in the same colony spreads slightly with time. Figure 2c represents the phases of the chosen oscillators from the two colonies (in red and black) on a circular 'phase plot'[16]. Each group of oscillators is also represented by a vector whose orientation angle gives the average phase and whose magnitude indicates the phase coherence (that is, its length is 1 when the oscillators are in phase, and 0 when the phase of the oscillators is uniformly randomly distributed). As we can see from this plot, the internal synchrony of each colony is close to 1 (>0.94) in the first days, and it is only slightly diminishing (>0.85) at the end of the experiment.

We can get some insight into the origins of this slow loss of synchronicity by examining more closely the spatial evolution of the phase in growing micro-colonies. In Fig. 3, oscillations in the cells from four micro-colonies are tracked as a function of time. The temporal evolution of the phase for some of the cell lines (see Methods) has been quantified as described in Fig. 2c. We represent the average phase of the circadian oscillator in each time interval by the colour of the overlaid temporal track. It is easy to see that the difference in phases of different cell lines does not notably decrease when they are driven closer to each other (Fig. 3, arrows). Of particular interest is the situation in which the phase of oscillations in two cell lines descending from the same initial progenitor cell differs, after a few cell divisions, by a measurable amount of ~30 degrees (see, for example, Fig. 3, pink arrow). This phase difference then persists through numerous division cycles even though both cell lines remain physically in close contact (Fig. 3). These observations confirm that any interactions between closely packed cells seem to have negligible effect on their relative phase of oscillations, at least for phase differences large enough to be detected (see Supplementary Information for an estimate of the detection limit of the coupling strength between oscillators).

The textbook definition of circadian clocks implies the existence of self-sustained oscillations, which can be entrained to the precise 24 h period by external cues (such as light and temperature), and which are temperature-compensated. These three requirements put definite constraints on the design of biochemical networks, which can implement circadian clocks in different multicellular organisms. Here we have shown that at least for cyanobacteria, these three requirements have to be supplemented by an additional one. In these small prokaryote cells, circadian oscillators are very resilient to

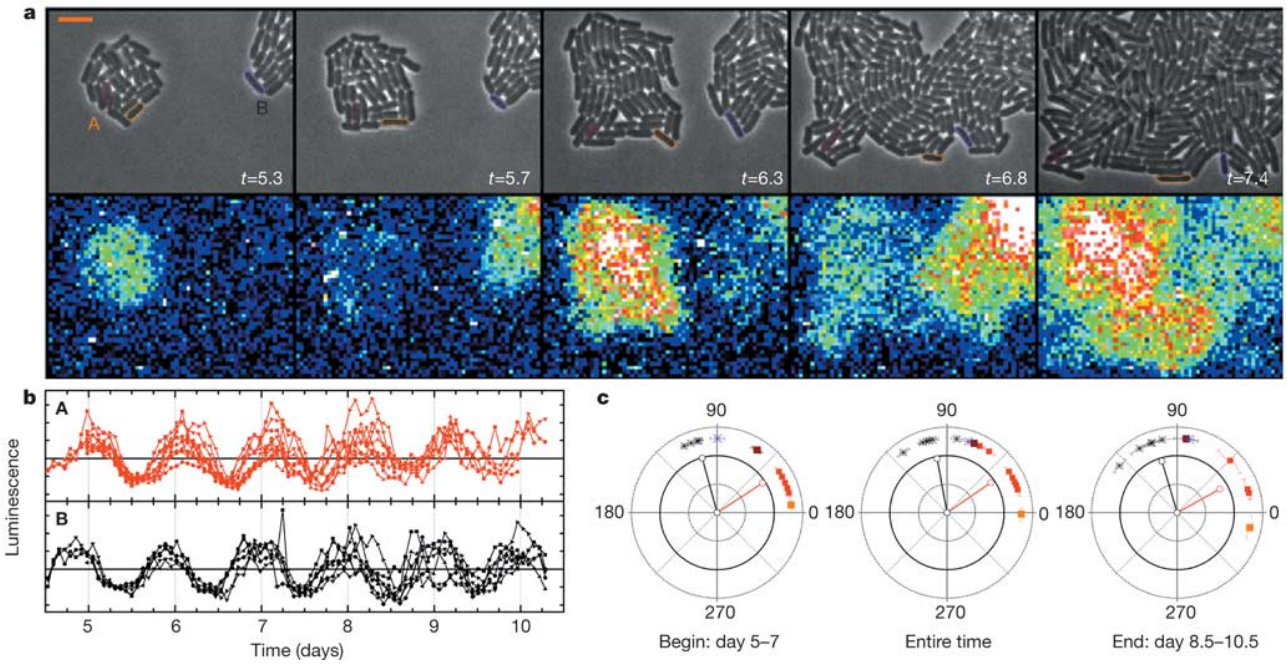

Figure 2 Growing micro-colonies of cyanobacteria, oscillating with different phases. **a**, Upper part shows the phase-contrast snapshots of colonies A and B; lower part shows the related bioluminescence images. Scale bar, 5 μm. **b**, Normalized density of bioluminescence of individual cyanobacterial cells. Each colour corresponds to the progeny from one of the initial cells: red line, colony A; black line, colony B. **c**, Phase of individual oscillators as a function of their original colony and their evolution in time: red square, colony A; asterisk, colony B. An example of the exact location for three of the cells tracked and their phase evolution is shown, marked by the corresponding coloured lines: magenta, orange and purple. The change of the phase in time was quantified by a fit over a different period of time: the first 2 days (days 5–7), the entire time (days 5–10.5) and the last 2 days of the measurement (days 8.5–10.5). The fit function is $\langle d(t)\rangle = B + A\cos(2\pi t/T_0 + \varphi)$, with $T_0 = 24.78$ h. The line segments in each graph, with corresponding colours, represent the resulting vector $\mathbf{P}_{res} = \sum \mathbf{P}_i$, where $\mathbf{P}_i$ is the unit vector whose orientation is the measured angle of the same colony cell *i*.

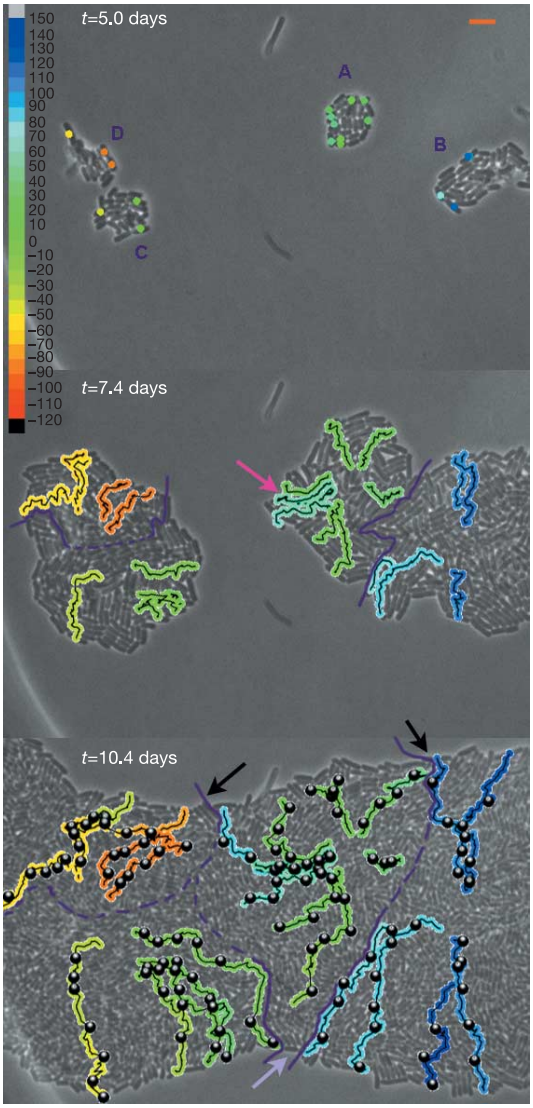

Figure 3 Temporal evolution of individual oscillators' phase is independent of close proximity. Snapshots of the four growing colonies (named A, B, C and D) in phase-contrast microscopy at three different times, *t*. Superposed are the tracks of the centre of gravity of each cell followed in time. The colour of each track is given by the phase of the circadian oscillation of the cell. Note that the colour of the interval 7–8.5 days of the time track represents the average phase of the given individual oscillator. The black filled dots represent a cell division event. The indigo lines show the precise (continuous line) or estimated (dashed line) boundary between the merging colonies. The arrows point to examples of spatially close cells oscillating with different phases. Scale bar, 5 μm.

perturbations associated with high intracellular noise and frequent cell divisions. The remarkable stability in time revealed in our experiments seems to be implemented at the single-cell level, and interactions between the oscillators in different cells seem to be negligible. This requirement of 'noise resistance' is a nontrivial one, and imposes strong constraints on any models of circadian biochemical networks[17–19]. □

Methods

Bioluminescence imaging

The detection system was chosen to have the highest quantum efficiency (QE) and a low electronic noise: a back-illuminated CCD system with 1,340 × 1,300 pixels, each of 20 μm × 20 μm, cooled to −100 °C and having QE, for the spectral range of the luciferase, higher than 85% (Roper Scientific-Princeton Instruments Camera, CT 1300B Cryotiger). For imaging cells with typical sizes of 2.3–6 μm, we used a high-magnification optical microscope with ×100 objective (Zeiss Axiovert 200 with a bottom port for a direct path to the detector and an oil contact lens Plan-Neofluar 100xPh3 numerical aperture = 1.3). The data acquisition was entirely automated with custom-made software, interfaced with the camera control software, Win View/32. For automatic focusing we used phase-contrast imaging (exposure 150 ms under low-intensity bright-field light). After each focusing we kept the system in dark for 2 min to avoid the phosphorescence of the intracellular chromophores. The bioluminescence images were subject to 3 × 3 binning of the pixels (to diminish the read-out noise of the camera). The growth of the cells was then assured by an exposure to fluorescent lamp light for 60–90 min (depending on the experiment) with a flux of ~100 $\mu E\,m^{-2}\,s^{-1}$ at the surface of the sample. One field of view, preceded by an automatic focusing, was taken every 95–125 min, and the length of one experiment was 1 to 2 weeks.

Cells and growth chamber

The transformed reporter strain[8] AMC412 was grown in BG-11 medium at 30 °C with 7.5 $\mu l\,ml^{-1}$ chloramphenicol and 5 $\mu g\,ml^{-1}$ spectinomycin, under 12 h light/12 h dark cycles for entrainment, then under continuous light (LL) for two different periods of time: 1 week and 2 months. The cells were then diluted in fresh media at 30 °C and grown again for 1 week in LL. The growth chambers for the microscope were made on 50 × 9 mm Petri dishes, with a 22 mm hole and a 25 mm No. 0 round coverslip (Erie Scientific) glued inside. Two to three microlitres of cells were spotted on the coverslip, coated with 100 μl of liquid 3% SeaPlaque low-melt agarose in media, and immediately covered and insulated with a transparent 0.4-μm-pore-size polyethylene terephthalate track-etched membrane (Falcon), and paraffin sealed. The Petri dish was then filled with 30 °C media, closed, incubated at 30 °C in LL for a few hours, and then installed under the microscope. In this way, the movement of the cells was highly restrained by the agarose gel, but all the cells retained homogeneous access to growth media, while a sufficiently transparent light pathway allowed phase-contrast microscopy.

Image and data analysis

Individual cells were manually identified on the phase-contrast images, from the final frame, backwards in time, to the first frame. A custom Matlab (MathWorks)-based software selected from the image the pixels corresponding to a given cell, extracted its size and position, and then in the bioluminescence image grouped the pixels 3 × 3 to identify the cell and to integrate its total bioluminescence. The cosmic rays, detected during the acquisition process, were easily discriminated owing to their high intensities when compared with the bacterial bioluminescence. The background value *bk*, constant for each bioluminescence frame, was taken as the maximum of the intensity histogram of all individual pixels chosen in a region devoid of cells. The density of bioluminescence per cell per pixel is calculated as: $d = \sum_{i=1}^{N_T} (\text{counts})_i / N_T - bk$, where N_T is the number of binned pixels describing the cell, and $(\text{counts})_i$ is the number of counts recorded from the pixel *i*. Note that both $(\text{counts})_i$ and N_T are random variables: $(\text{counts})_i$ owing to the Poisson statistics of photons and the noise of the CCD camera, and N_T because of the sampling of the continuous contour of a cell with a small number of pixels (see Supplementary Information). All fits have been done using the Levenberg–Marquardt χ^2 minimization algorithm with Origin (OriginLab) software and the uncertainty of parameters is the standard deviation obtained from the curvature of the χ^2 around its minimum.

The choice of individual cells for study was restricted to those growing essentially in a single two-dimensional layer. Note that if one cell lies on top of another cell, the bioluminescence information becomes irrelevant at the single-cell level and its track has to be aborted. Therefore, the cell lines chosen were those having the longest history in a single monolayer. This constraint was more restrictive in the last experiment. The number of cells grew ~50–100 times (that is, ~6 division cycles) and most of the cells soon after division were caught in multilayered colonies. At the interface between two merging colonies, the stacking up is enhanced and the cells available for tracking were typically the few that remained at the common outside border of both colonies.

Received 23 November 2003; accepted 30 March 2004; doi:10.1038/nature02533.

1. Young, M. W. & Kay, S. A. Time zones: a comparative genetics of circadian clocks. *Nature Rev. Genet.* **2,** 702–715 (2001).
2. Barkai, N. & Leibler, S. Circadian clocks limited by noise. *Nature* **403,** 267–268 (2000).
3. Pikovsky, A., Rosenblum, M. & Kurths, J. *Synchronization: A Universal Concept in Nonlinear Sciences* (Cambridge Univ. Press, Cambridge, 2001).
4. Liu, C., Weaver, D. R., Strogatz, S. H. & Reppert, S. M. Cellular construction of a circadian clock: period determination in the suprachiasmatic nuclei. *Cell* **91,** 855–860 (1997).
5. Yamaguchi, S. *et al.* Synchronization of cellular clocks in the suprachiasmatic nucleus. *Science* **302,** 1408–1412 (2003).
6. Kondo, T. *et al.* Circadian rhythms in prokaryotes: luciferase as a reporter of circadian gene expression in cyanobacteria. *Proc. Natl Acad. Sci. USA* **90,** 5672–5676 (1993).
7. Liu, Y. *et al.* Circadian orchestration of gene expression in cyanobacteria. *Genes Dev.* **9,** 1469–1478 (1995).
8. Katayama, M., Tsinoremas, N. F., Kondo, T. & Golden, S. S. *cpmA*, a gene involved in an output pathway of the cyanobacterial circadian system. *J. Bacteriol.* **181,** 3516–3524 (1999).
9. Tsinoremas, N. F., Schaefer, M. R. & Golden, S. S. Blue and red light reversibly control *psbA* expression in the cyanobacterium *Synechococcus* sp. strain PCC 7942. *J. Biol. Chem.* **269,** 16143–16147 (1994).
10. Kondo, T. *et al.* Circadian rhythms in rapidly dividing cyanobacteria. *Science* **275,** 224–227 (1997).
11. Mori, T. & Johnson, C. H. Independence of circadian timing from cell division in cyanobacteria. *J. Bacteriol.* **183,** 2439–2444 (2001).
12. Mori, T., Binder, B. & Johnson, C. H. Circadian gating of cell division in cyanobacteria growing with average doubling times of less than 24 hours. *Proc. Natl Acad. Sci. USA* **93,** 10183–10188 (1996).
13. Gaspard, P. The correlation time of mesoscopic chemical clocks. *J. Chem. Phys.* **117,** 8905–8916 (2002).
14. Elowitz, M. B., Levine, A. J., Siggia, E. D. & Swain, P. S. Stochastic gene expression in a single cell. *Science* **297,** 1183–1186 (2002).

15. Kiss, I. Z., Zhai, Y. & Hudson, J. L. Emerging coherence in a population of chemical oscillators. *Science* **296,** 1676–1678 (2002).
16. Levine, J. D., Funes, P., Dowse, H. B. & Hall, J. C. Resetting the circadian clock by social experience in *Drosophila melanogaster. Science* **298,** 2010–2012 (2002).
17. Winfree, A. T. *The Geometry of Biological Time*, 2nd edn (Springer, New York, 2001).
18. Goldbeter, A. Computational approaches to cellular rhythms. *Nature* **420,** 238–245 (2002).
19. Gonze, D., Halloy, J. & Goldbeter, A. Robustness of circadian rhythms with respect to molecular noise. *Proc. Natl Acad. Sci. USA* **99,** 673–678 (2002).

Supplementary Information accompanies the paper on **www.nature.com/nature**.

Acknowledgements We thank S. Golden for the AMC412 strain and for advice, D. Peoples for advice and technical assistance, B. Houchmandzadeh, J. Paulsson, J. Vilar, C. Weitz and M. Young for discussions, and N. Questembert-Balaban, E. Kussell and M. Vallade for comments on the manuscript. This work was supported partially by Princeton University through the Lewis Thomas Fellowship (I.M.), the National Institutes of Health, the Howard Hughes Medical Institute and the Centre National de Recherche Scientifique through an ATIP and an AC 'Dynamique et réactivité des assemblages biologiques'.

Competing interests statement The authors declare that they have no competing financial interests.

Correspondence and requests for materials should be addressed to I.M. (imihalce@spectro.ujf-grenoble.fr).

Evolutionary changes in *cis* and *trans* gene regulation

Patricia J. Wittkopp, Belinda K. Haerum & Andrew G. Clark

Department of Molecular Biology and Genetics, Cornell University, Ithaca, New York 14853, USA

Differences in gene expression are central to evolution. Such differences can arise from *cis*-regulatory changes that affect transcription initiation, transcription rate and/or transcript stability in an allele-specific manner, or from *trans*-regulatory changes that modify the activity or expression of factors that interact with *cis*-regulatory sequences[1,2]. Both *cis*- and *trans*-regulatory changes contribute to divergent gene expression, but their respective contributions remain largely unknown[3]. Here we examine the distribution of *cis*- and *trans*-regulatory changes underlying expression differences between closely related *Drosophila* species, *D. melanogaster* and *D. simulans*, and show functional *cis*-regulatory differences by comparing the relative abundance of species-specific transcripts in F_1 hybrids[4,5]. Differences in *trans*-regulatory activity were inferred by comparing the ratio of allelic expression in hybrids with the ratio of gene expression between species. Of 29 genes with interspecific expression differences, 28 had differences in *cis*-regulation, and these changes were sufficient to explain expression divergence for about half of the genes. *Trans*-regulatory differences affected 55% (16 of 29) of genes, and were always accompanied by *cis*-regulatory changes. These data indicate that interspecific expression differences are not caused by select *trans*-regulatory changes with widespread effects, but rather by many *cis*-acting changes spread throughout the genome.

D. melanogaster and *D. simulans* diverged about 2.5 Myr ago[6], yet are still able to mate and produce viable (but sterile) offspring. Their compatibility allowed us to identify *cis*- and *trans*-regulatory changes by comparing the regulation of species-specific alleles in a common, hybrid genetic background. Differential expression of two alleles in the same cellular environment indicates functional *cis*-regulatory differences[4,5,7]; thus, asymmetric allelic expression in F_1 hybrids implies *cis*-regulatory divergence. If *trans*-regulation diverges between species, the collection of *trans*-acting factors in hybrids will be different from that in one or both of the parental species. As a result, the relative allelic expression in hybrids will differ from the relative gene expression between species. *Trans*-regulatory divergence was inferred for any gene with significant differences in the ratio of species-specific transcripts between F_1 hybrids and the parental species.

To measure the relative abundances of species-specific transcripts, we analysed RNA and DNA, extracted separately from pools of female flies containing either 14 F_1 hybrids or 7 *D. melanogaster* and 7 *D. simulans* individuals (Fig. 1a). Four complementary DNA samples were generated from each RNA extraction and used to measure the relative abundance of species-specific transcripts. At least two replicate hybrid pools (eight cDNA measurements in total) and four replicate parental pools (16 cDNA measurements in total) were analysed for each gene. The ratio of *D. melanogaster* to *D. simulans* alleles was also measured in genomic DNA from each pool in duplicate and used to correct cDNA ratios for allelic differences in extraction and/or amplification (Supplementary Information). For each gene, the ratio of expression between species (designated Mel/Sim) and the ratio of species-specific transcripts in F_1 hybrids (designated Mel_{F1}/Sim_{F1}) were quantified, normalized and averaged across replicate pools.

Pyrosequencing[8] was used to measure the relative abundance of *D. melanogaster* and *D. simulans* alleles directly in cDNA and DNA samples. A single nucleotide difference that distinguished the species-specific transcripts was identified for each gene, and polymerase chain reaction (PCR) primers were used to amplify a region of DNA containing the divergent site (Fig. 1b). After denaturing the PCR products, an internal primer ('Pyro-reverse' in Fig. 1b) was annealed and extended one base at a time in a Pyrosequencing

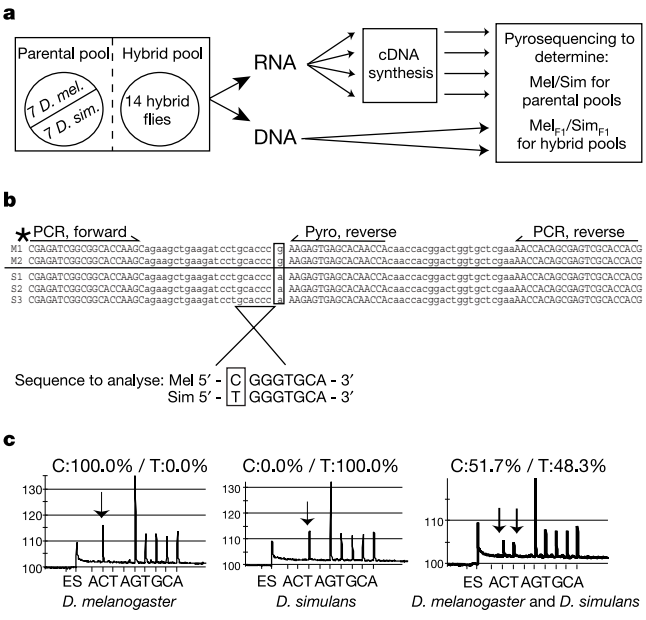

Figure 1 Pyrosequencing[8] measures allelic gene expression. **a**, Overview of sample collection. **b**, Example assay of CG14770. Aligned coding sequences from *D. melanogaster* (M1, M2) and *D. simulans* (S1–S3) identify transcribed fixed differences (box). The location of PCR and Pyrosequencing primers are shown with an asterisk indicating the biotinylated PCR primer. **c**, Pyrosequencing produces a pyrogram with peaks whose height is directly proportional to the quantity of nucleotide added to the extending Pyrosequencing primer. Pyrograms from reactions using genomic DNA from *D. melanogaster* (left), *D. simulans* (middle), and both species (right) are shown. Arrows indicate peaks reflecting nucleotide incorporation at the divergent site. ES indicates the addition of enzymes and substrate, respectively.